Genome editing in the mouse brain with minimally immunogenic Cas9 RNPs

Elizabeth C. Stahl[1-3], Jennifer K. Sabo[1*], Min Hyung Kang[1,5], Ryan Allen[1], Elizabeth Applegate[1], Shin Eui Kim[1], Mika Kwon[1,3], Anmol Seth[1,3], Nicholas Lemus[1,3], Viviana Salinas-Rios[1], Katarzyna Soczek[1-3], Marena Trinidad[1], Linda T. Vo[1#], Chris Jeans[2], Anna Wozniak[4], Timothy Morris[4], Athen Kimberlin[4], Thomas Foti[4], David F. Savage[1,3,5] and Jennifer A. Doudna[1-3,5-8†]

[1]Innovative Genomics Institute, University of California, Berkeley, California 94720, USA; [2]California Institute for Quantitative Biosciences (QB3), University of California, Berkeley, California 94720, USA; [3]Department of Molecular and Cell Biology, University of California, Berkeley, California 94720, USA; [4]Aldevron LLC, Madison, Wisconsin 53719, USA; [5]Howard Hughes Medical Institute, University of California, Berkeley, California 94720, USA; [6]Department of Chemistry, University of California, Berkeley, CA, USA 94720; [7]MBIB Division, Lawrence Berkeley National Laboratory, Berkeley, California 94720, USA; [8]Gladstone Institutes, University of California, San Francisco, CA 94114

†Correspondence: doudna@berkeley.edu

*Current address: Scribe Therapeutics Inc. Alameda, CA, 94501

[#]Current address: Third Rock Ventures, Boston, MA, 02116

Abstract

Transient delivery of CRISPR-Cas9 ribonucleoproteins (RNPs) into the central nervous system (CNS) for therapeutic genome editing could avoid limitations of viral vector-based delivery including cargo capacity, immunogenicity, and cost. Here we tested the ability of cell penetrant Cas9 RNPs to edit the mouse striatum when introduced using a convection enhanced delivery system. These transient Cas9 RNPs showed greater local editing of neurons and reduced adaptive immune responses relative to Cas9 delivered using AAV serotype 9. The production of ultra-low-endotoxin Cas9 protein manufactured at scale further improved innate immunity. We conclude that injection-based delivery of minimally immunogenic CRISPR genome editing RNPs into the CNS provides a valuable alternative to virus-mediated genome editing.

Introduction

Editing somatic cells directly *in vivo* is anticipated to be the next wave of therapeutics for many genetic diseases, especially those affecting the central nervous system (CNS)[1,2]. Clustered regularly interspaced short palindromic repeats (CRISPR) is a revolutionary tool adapted from bacterial immune systems for genome editing[3–5]. To achieve gene disruption, the functional endonuclease, Cas9, is directed by a guide RNA to a target site in DNA to generate a double strand break leading to insertions and deletions (indels). Unfortunately, despite many genetic disease indications, the brain remains a challenging target for genome editing.

To circumvent the blood-brain barrier (BBB), most genomic medicines rely on direct intracranial injection of viral vectors encoding the transgene of interest. Viral vectors, such as recombinant adeno-associated virus (AAV), have had great success in gene therapy and are less immunogenic than most viral vectors, however, they require re-manufacturing for each target and are hindered by costly production scale up. Additionally, AAV has a limited DNA packaging capacity and is associated with immunogenicity in the brain from both the vector and expression of foreign transgenes[6–9]. Although the brain has been considered an immune-privileged site, green fluorescent protein can induce a strong inflammatory response and neuronal cell death three weeks after injection with AAV serotype 9 has been reported[6–9]. Additionally, Cas9-specific immune responses have been elicited following AAV delivery in mice[10–12] and pre-existing cellular and humoral immunity to Cas9 and AAVs are documented in humans[13–18]. Despite these drawbacks, AAVs are the most clinically relevant delivery systems currently in use for the CNS.

The development of transient, non-viral delivery systems that can effectively edit neurons throughout the brain with minimal immunogenicity would greatly facilitate future clinical applications. Previously, we developed cell penetrating Cas9 ribonucleoproteins (RNPs) capable of genome editing in mouse neurons both *in vitro* and *in vivo*[19]. To enable self-delivery of the Cas9 RNPs, four repeats of the positively charged Simian vacuolating virus 40 nuclear localization sequences (SV40-NLS) were fused to the N-terminus along with two repeats to the C-terminus of

Cas9, a strategy that was also reported to enable delivery of zinc-finger nucleases[20]. Using a single guide to turn on the tdTomato reporter from the lox-stop-lox (LSL-Ai9[21]) mouse, we reported edited striatal volume of approximately 1.5mm^3 [19].

Here we report further optimization of cell penetrant Cas9 RNPs, demonstrating efficacy in human primary cells and improved editing of the mouse striatum using a convection enhanced delivery CED system. We compared the transient RNP complexes to AAV serotype 9 for Cas9 delivery to the CNS, to measure both editing efficiency and the host immune response. We found that cell penetrant Cas9-RNPs edited significantly more neurons within a given area than Cas9-AAVs but were less efficient at diffusing throughout the brain and cerebrospinal fluid. Both groups elicited humoral responses, but anti-capsid antibodies in the Cas9-AAV group persisted at high levels out to 90-days and AAV treated brains were associated with significantly elevated *Cd3e* gene expression at four weeks, suggesting an ongoing adaptive immune response. Cas9-RNP treated brains showed acute microglial activation that was mitigated by reducing endotoxin levels during protein manufacturing scale up. Studies suggest that correcting pathological mutations in 20-30% of striatal neurons expressing mutant huntingtin protein would be sufficient to significantly improve the disease pathology[22]. Therefore, Cas9 RNPs are a promising strategy for localized therapeutic intervention in neurological disorders to address current limitations of viral delivery.

Results

Development of Cas9 cell penetrant RNP and AAV to measure genome editing with the tdTomato reporter system

Creating a large deletion in the lox-stop-lox cassette in Ai9 mice with a single guide RNA (sgRNA) enables expression of tdTomato and efficient quantification of editing by fluorescent read out (Figure S1A). Cas9 from *Streptococcus pyogenes* (engineered with four copies of SV40 NLS on the N-terminus and two copies on the C-terminus (4x-SpyCas9-2x) to be cell penetrant) was first produced from recombinant *E. coli* in a laboratory setting, using a low-endotoxin method. Editing efficiency of the RNP was compared to Cas9 delivered by recombinant adeno-associated virus (AAV) (Figure 1A-B). Since SpyCas9 cannot fit within a single AAV with its guide RNA, we used clinically relevant AAV-SauCas9-sgRNA (derived from *Staphylococcus aureus*)[23–25]. AAV serotype 9 was produced using a baculovirus transfected into Sf9 insect cells[26,27]. To control for differences in the Cas9 orthologues, cell penetrant 4x-SauCas9-2x protein was also produced following the same expression and purification methods as 4x-SpyCas9-2x. Due to differences in PAM requirements between the two Cas9 orthologues (SpyCas9 NGG, SauCas9 NNGRRT), a new guide was designed for SauCas9 to target the tdTomato locus (Figure S1B).

We confirmed editing in neural precursor cells (NPCs) isolated from embryonic day 13.5 Ai9 mice with all constructs *in vitro* (Figure S1C-E). Interestingly, we observed greater editing of mouse NPCs with SauCas9 when delivered as cell penetrant RNP compared to AAV, as AAV preps often include empty capsids (Figure S1F) and require high multiplicity of infection for efficient transduction in cell culture[28,29]. The 4x-SauCas9-2x was slightly less efficacious when editing mouse NPCs compared to 4x-SpyCas9-2x, which could be explained in part by differences in the guide RNAs.

To further examine the potential for cell penetrant Cas9 RNPs to edit difficult cells *in vitro*, we tested delivery and editing with 4x-SpyCas9-2x in human neural precursor cells derived from induced pluripotent stem cells (iPSCs)[30–32]. Human NPCs were treated with pre-formed RNPs

using an established guide RNA targeting EMX1[33]. In human cells, we detected 10x higher rates of editing with 4x-SpyCas9-2x compared to standard RNP delivered with commercial transfection reagents (Figure S2A-B).

Cas9 RNPs result in modest editing of brain parenchyma following delivery into cerebrospinal fluid

To determine the optimal route of delivery for Cas9 RNPs into the mouse CNS, we tested intraparenchymal injections into the striatum, as well as injection into the cerebrospinal fluid (CSF), including intrathecal (IT) and intracerebroventricular (ICV) routes. Following IT injection of cell penetrant RNPs, we observed edited glial cells and neurons in the cortex and striatum of one hemisphere, but no editing within the spinal cord (Figure S3A). Following ICV injection of Cas9 RNPs in neonatal p0 mice, we observed tdTomato^{+} cells in the subventricular zone and white matter, including glial cells and neural stem/progenitor cells expressing Ki67 and DCX evaluated three weeks after delivery (Figure S3B-C). Editing post-ICV injection in adult mice was restricted to the cells within the lateral ventricles, choroid plexus, subventricular zone, and hippocampus in a subset of mice (Figure S3D). In all cases, the total number of edited cells with RNP delivery into the CSF was lower than with direct intraparenchymal injection.

Therefore, we sought to further improve upon intraparenchymal injections using a convection enhanced delivery system (CED), which consists of silicon tubing fused into a blunt needle to create a cannulated step (Figure S4A). CED has been reported to increase the diffusion of molecules in the brain, including AAV, which is particularly important in large animal models and humans[34,35]. While CED did not significantly improve the volume of edited striatal tissue compared to the non-cannulated blunt needle with 4x-SpyCas9-2x RNP (Figure S4B), CED did significantly reduce reflux of RNP from the needle-injection track (Figure 1D). Furthermore, tdTomato^{+} neurons edited by Cas9-RNPs within the striatum were observed to extend along the

basal ganglia circuit into the globus pallidus and substantia nigra along the anterior-posterior axis (Figure 1C-E).

Convection enhanced delivery of Cas9 RNPs and AAVs mediates robust editing in the mouse striatum

Using bilateral CED injections into the striatum, we compared edited tissue volume using the 4x-SpyCas9-2x RNP, 4x-SauCas9-2x RNP, and AAV9-SauCas9-sgRNA in adult Ai9 mice at three weeks post-injection. Despite performing well *in vitro*, 4x-SauCas9-2x RNPs underperformed *in vivo* when tested at two different doses and additional NLS configurations (Figure S5). Therefore, we performed our primary comparison between 4x-SpyCas9-2x RNP (hereafter referred to as Cas9-RNP) and AAV9-SauCas9-sgRNA (hereafter referred to as Cas9-AAV).

Overall, we observed diffuse tdTomato signal throughout the striatum and cortex in the Cas9-AAV group, whereas we observed more intense tdTomato signal emanating from the injection site with the Cas9-RNP group (Figure 1F, Figure S6C). We tested several doses of Cas9-RNP by keeping the injection volume constant and increasing the concentration of the RNP in solution from 10µM to 100µM. There was no significant difference in the edited striatal volume when delivering RNPs in this concentration range (Figure 1H) and editing levels seemed to decrease slightly at 50µM and 100µM compared to the 10µM and 25µM groups. We chose the 25µM concentration (4.15 mg/mL or approximately 1.75 mg/kg Cas9) group for further study as it had the highest maximal editing rate. Above 25µM in the RNP group, we observed a decrease in NeuN staining and an increase in GFAP staining out to 90-days in the Cas9-RNP group, suggesting dose-limiting effects (Figure 1G).

At both 21 and 90-days post-injection, the Cas9-AAV group outperformed the Cas9-RNP group when quantifying total edited striatal volume ($n=8$ at 21-days, $n=4$ at 90-days, $p<0.05$,

Figure 1I). The volume of edited cells was relatively stable in the Cas9-AAV group between 21 and 90-days at approximately 47 ± 3% (covering approximately 13.4 mm^3 of striatum), while the Cas9-RNP group had editing levels of 22 ± 3% (approximately 6.2 mm^3 of striatum) between 21 and 90-days (increased from previous report of editing 1.5mm^3 striatal volume[19]). Edited cells were observed further along the rostral-caudal axis (-2.12 mm to 2.5 mm relative to Bregma), demonstrating better diffusion of the editor away from the injection site in the Cas9-AAV group (Figure S6D-E).

Since large deletions in the tdTomato locus make on-target editing difficult to assess using short-read next-generation sequencing (NGS), we developed an NHEJ droplet digital PCR assay (ddPCR) to measure drop-off of HEX-labeled probes over the cut sites, in relation to distal reference FAM-labeled probes. Genomic DNA was isolated from 2-mm thick sections of each injected hemisphere, covering multiple brain sub-structures. Loss of the HEX probe reached 2 ± 1% in the Cas9-RNP group and 15 ± 10% in the Cas9-AAV group, indicating edited alleles, when measured at 28-days (Figure S5G).

We also quantified the percentage of edited $NeuN^+$ neurons within the $tdTomato^+$ region of interest (ROI) per hemisphere between Cas9-AAV and Cas9-RNP at the 21-day timepoint. We found that Cas9-RNP edited significantly more $NeuN^+$ neurons per ROI (36 ± 10%) compared to Cas9-AAV (20 ± 2%) (Figure 1J, n=6-8 injections, $p<0.05$). Within the ROI, neurons were the most frequently edited cell type in both groups, including $DARPP32^+$ medium spiny neurons (Figure S6). Additionally editing of $ALDH1L1^+$ and $OLIG2^+$ glial cells was noted in both groups (approximately 2% of edited cells within the ROI in the Cas9-RNP group and 8% of cells in the Cas9-AAV group). Therefore, Cas9-RNPs generated higher rates of edited neurons within a given area and demonstrated a preference for editing neurons over glial cells, as observed previously[19], compared to Cas9-AAV (Figure S6A-B).

Comparison of local and peripheral immune response between Cas9 RNPs and AAVs in the Ai9 reporter mouse

We next examined the local and peripheral immune response following delivery of Cas9 RNPs and AAVs into the brain. Using immunofluorescent staining for Iba1 (Figure 2A), we observed similar numbers of microglia between the groups, but increased staining intensity in the 25µM Cas9-RNP group leading to a significant increase in percent $Iba1^+$ area from sham-treated animals (Figure 2B, n=6 replicates, one-way ANOVA, $p<0.05$). Staining for CD45 showed dim expression on $Iba1^+$ microglia and high expression on $CD3^+$ T-cells, which were slightly increased in the 25µM Cas9-RNP group compared to the sham and Cas9-AAV, but not significant different, at three weeks post-injection (Figure 2C-D, n=6-12 replicates).

In addition to the immune response at the local site of injection, circulating IgG antibodies were measured at 28 and 90-days post-injection. We found that sham-treated animals had no pre-existing antibodies to either SpyCas9, SauCas9, nor AAV9 capsids. At 28-days following striatal injection, there was a 1.6e4-fold increase in anti-SpyCas9 IgG in the 25μM Cas9-RNP group, a 1.3e4-fold increase in anti-AAV9 capsid IgG in the Cas9-AAV group, and an 8.9e1-fold increase in anti-SauCas9 IgG in the Cas9-AAV group (i.e., humoral response against transgene) (Figure 2E, n=3-5 biological replicates). No cross-reactivity was observed between orthologue RNPs, as described previously[11], nor were any anti-AAV capsid antibodies detected in the RNP group. At 90-days, the levels of IgG fell to a 5.4e2-fold increase in the 25µM Cas9 RNP group and 1.2e4-fold increase in the Cas9 AAV group from the sham controls, demonstrating greater maintenance of systemic antibodies against the capsid in the AAV group.

The cellular and humoral immune response to Cas9 RNPs was dose-dependent and a significant increase in $CD45^+$ cells was observed at the 100µM RNP dose compared to sham, Cas9-AAV, and Cas9-RNP at 25µM (Figure S7). Cas9-reactive cells were also identified in the

spleen by interferon-gamma (IFN-γ) ELISpot assay (Figure S7E) at both 25µM and 100µM doses of Cas9-RNPs, but not in sham treated animals.

Since the mice had no pre-existing antibodies to SpyCas9, we tested how the immune response would differ in the RNP group by first exposing the mice to a single subcutaneous injection of 4x-SpyCas9-2x protein and adjuvant (AddaVax™) four-weeks prior to stereotaxic surgery with Cas9-RNPs. We found that pre-exposing the mice to Cas9 had a synergistic effect on both serum IgG and activation of IFN-γ^+ cells in the spleen (Figure S7F-I). Mice that received surgery maintained tdTomato$^+$ cells in the brain to the measured time point. Additional studies using this immunization strategy may help to further characterize the immune response to Cas9-RNPs by modeling pre-existing immunity relevant to humans.

Finally, we measured gene expression changes in mice that received Cas9-RNP and AAV at 3 and 28-days post-injection using RT-qPCR. At three days, the Cas9-AAV group had a modest but significant increase in *Fas* (1.19-fold) and *FasI* (1.85-fold) compared to the sham group (Figure 2F). At 28-days post-injection, both Cas9-RNP and -AAV had a significant increase in *Fas* (1.61 and 1.89-fold respectively). In addition, the Cas9-AAV group had a significant increase in *CD3e* gene expression (5.45-fold, n=4 replicates, $p<0.05$), closely followed by *CD8a* (2.06-fold, ns, $p=0.06$), while Cas9-RNP had a slight but non-significant increase in *CD3e* (2.15-fold, ns, $p=0.06$), compared to the sham group.

There were no detectable off-target editing events at 1 and 4-months post-injection in any of the experimental groups at the evaluated off-target sites (Figure S8A-C). In the Cas9-AAV group, the Cas9 transgene was expressed in the brain out to 4-months, the last tested time point, as expected (Figure S8D). Additionally, few genes were differentially expressed between the groups at 4-months, except for *Fas* (1.54-fold), which was significantly elevated in the Cas9-AAV group compared to the sham (Figure S8E-F). We used long read sequencing to examine whether any fragments of the viral genome had been integrated near the cut site in the tdTomato locus,

as previously reported[36–39]. We also observed partial integrations of viral fragments in our amplicon, although our *in vivo* editing rates and sequencing depth were relatively low (Figure S9).

We concluded that delivery of Cas9 to the brain was well-tolerated in naïve mice. However, the increase of Iba1$^+$ cells near tdTomato$^+$ cells in the striatum in the 25µM Cas9-RNP group raised the question of whether the response was due to Cas9 itself or impurities within the protein product. We hypothesized that the local immune response may be due to endotoxins from *E. coli* in the RNP complexes.

Production and testing of ultra-low endotoxin 4x-SpyCas9-2x protein

To examine the impact of endotoxin on the immune response to RNPs, we partnered with a commercial producer of Cas9 protein and were able to significantly scale up manufacturing to produce a large quantity of ultra-low endotoxin 4x-SpyCas9-2x protein using an industrial tag-free expression and purification system (Figure 3A).

Using the limulus amebocyte lysate (LAL) assay, we measured an endotoxin concentration of 0.035 EU/mg in the industrial-produced protein compared to 0.2 EU/mg in the lab-produced protein (Figure S10A). Interestingly, using the same assay, we found that guide RNA could be an unexpected source of endotoxin contamination. Endotoxin was present in at least three unopened vials of lyophilized RNA that had been stored at -80°C from a 2018 lot, but not in a more recently purchased lot from the same vendor when resuspended simultaneously (Figure S10A-C). To rule out false positives due to reaction of LAL with beta-glucans, we performed the Recombinant Factor C (rFC) assay. The guide RNAs had a similar level of endotoxins between the LAL and rFC assays, demonstrating the positive signal was from contamination with endotoxin and not beta-glucans (Figure S10D-E).

To measure the physiological impact of endotoxin in our samples, we used HEK293 cells that were engineered to produce secreted embryonic alkaline phosphatase (SEAP) downstream

of NF-κB activation resulting from human toll-like receptor 4 stimulation (hTLR4) with endotoxin/lipopolysaccharide (LPS, Figure S11A-E). The lab-produced protein stimulated NF-κB in HEK293 cells significantly greater than the industrial produced protein ($p<0.01$, unpaired t-test). Treatment with the industrially produced protein led to similar levels of SEAP between hTLR4 cells and the parental cell line (Null2), demonstrating that most of the NF-κB stimulation was downstream of other pattern-recognition receptors (such as TLR3, TLR5, or nucleotide-binding oligomerization domain-containing protein 1 (NOD-1) activation) and not due to LPS signaling through hTLR4 (Figure S11A-E). When combined with sg298 from the 2018 or 2022 lot, absorbance levels of SEAP further increased in RNP complexes made with lab produced protein, while the industrial protein with either guide did not induce a response (Figure S11F). Furthermore, guide RNA alone did not stimulate NF-κB in HEK293 cells (Figure S11D).

Finally, we measured endotoxins in the "optimized" formulation of RNPs, comprised of the industrially produced 4x-SpyCas9-2x protein and 2022 sgRNA, using the LAL assay. Estimating delivery of 10µL per mouse, the endotoxin burden was 0.44 EU/kg when RNPs were formulated at 25µM. These data suggest that RNPs could be delivered below the 0.2 EU/kg FDA threshold for intrathecal delivery[40] when formulated at 10µM without significant loss of editing (Figure 3B and Figure 1H).

Optimized RNP formulation reduces immune response

We performed CED bilateral intrastriatal injections to test if reducing endotoxins would improve the host immune response to RNPs *in vivo*. In this experiment, we compared the optimized RNP formulation (industrially produced 4x-SpyCas9-2x NLS protein with sg298 2022) to the standard formulation used in Figures 1 and 2 (laboratory produced 4x-SpyCas9-2x NLS protein with sg298 2018) at 25µM. The standard RNP induced a significant increase in $Iba1^+$ area, consistent with our previous measurements (Figure 3C and Figure 1A); however, the optimized

Cas9-RNP formulation did not induce microglial activation. Additionally, there was no increase in $CD45^+$ and $CD3^+$ cells from the sham in the optimized RNP group (Figure 3D). Of note, the standard RNP edited an average of 31 ± 3% striatal volume (greater than values reported in Figure 1), while the optimized RNP edited an average of 23 ± 8% striatal volume (Figure 3F). Interestingly, the standard RNP also lead to significantly greater anti-Cas9 IgG responses at three-weeks post-injection, possibly due to endotoxin boosting the adaptive immune response (Figure 3G). Taken together, we found that reducing endotoxins in both the guide RNA and protein components of the RNP leads to a reduced innate immune response, comparable to the sham and AAV9 groups, while maintaining high on-target editing. Furthermore, cell penetrant Cas9 proteins are more amenable than AAVs for expedited manufacturing of large quantities suitable for *in vivo* experiments.

In conclusion, our results establish complementary genome editing and immunogenicity outcomes between the two tested Cas9 delivery strategies. To enable editing of multiple sub-brain structures, glial cells, and delivery through the CSF, AAV serotype 9 is preferred. To enable high levels of editing in neurons within a localized brain sub-structure, minimizing adaptive immune responses, and enabling manufacturing scale up, the RNP is preferred.

Discussion

In the present study, we demonstrate that cell penetrant Cas9 RNPs edit a therapeutically relevant volume of the mouse striatum using convection enhanced delivery. Furthermore, the 4x-NLS modification enables self-delivery of Cas9 orthologous proteins *in vitro* to both mouse and human cells, demonstrating cross-species compatibility of the system for the first time. We also show that Cas9 RNPs have dose-dependent effects on the immune response, which can be mitigated by using ultra-low endotoxin protein produced in an industrial non-GMP setting. These experiments are informative for the design of future therapeutic applications of Cas9 RNP editors in mice and larger animal models.

Several studies have reported non-viral delivery of Cas9 into the mouse brain. The "CRISPR-Gold" Cas9 nanoparticle delivery system induced 14% edited glial cells near the injection site, sufficient to reduce repetitive behaviors in a mouse model of fragile X syndrome[41]. Additionally, incubating RNPs with R7L10, an arginine and leucine rich cationic peptide, induced 45% indels in the CA3 region of the hippocampus, leading to behavioral improvements in an Alzheimer's disease mouse model[42]. Furthermore, editing of DARPP-32 medium spiny neurons in the striatum was achieved using RNPs packaged in biodegradable PEGylated nanocapsules[43]. Interestingly these nanocapsules had a neutral charge, while our 4x-Cas9-2x NLS RNPs have a net-positive charge, suggesting the mechanism of entry may differ between the two strategies.

Systemic delivery of genome editors with glucose-conjugated silica nanoparticles and AAV9 can lead to modest levels of editing in the brain, sufficient for therapeutic benefit [44,45]. In this study, we found that the Cas9-AAV distributed further through the brain than Cas9-RNPs, although the RNP delivery approach was more effective for high levels of localized neuronal editing. It is important to note that expression of the tdTomato protein in the Ai9 mouse model significantly underreports the actual genome editing efficiency, as double strand breaks that result in small indels are not sufficient to turn on the reporter[19]. Despite the need for direct injection, the simplicity of the cell penetrant protein makes it ideal from a manufacturing perspective compared to other nanoparticle formulations. The cell penetrant RNP could be further mixed with polymers, such as polyethylene glycol (PEG)[46], to improve biodistribution in the future.

We hypothesized that cell penetrant Cas9-RNPs would be less immunogenic than Cas9-AAVs due to their transient expression. As the dose of 4x-SpyCas9-2x RNPs increased from 25µM to 100µM, there was an increase in $CD45^+$ and $GFAP^+$ cells, and a decrease in $NeuN^+$ cells. As such, subsequent experiments were performed at 25µM, which was well-tolerated and resulted in similar levels of editing as the higher dose. The 25µM Cas9-RNP led to lower levels of vehicle-specific antibodies by 90-days post-injection compared to AAVs and did not upregulate

329 gene signatures of T-cells at 28-days as measured by RT-qPCR, supporting our hypothesis.
330 Reducing endotoxin in both the Cas9 protein and guide RNA prevented microglial reactions and
331 reduced humoral responses at 21-days.

332 In the Cas9-AAV group, few immune cells (CD45, Iba1, or CD3) were observed in the
333 striatum by immunostaining, however *CD3e* gene expression was significantly upregulated in
334 explanted tissue, closely followed by an increase in *CD8a*. This finding could indicate
335 accumulation of cytotoxic T-cells trafficking into the parenchyma from the blood vessels or
336 ventricles. Additionally, no changes in NeuN, GFAP, and CD45 expression were observed in the
337 Cas9-AAV group out to 4 months, demonstrating that the AAV delivery strategy was well-tolerated
338 overall in naïve mice. A study by Li et al. found that mice immunized against SauCas9 with
339 Freund's adjuvant one week prior to intravenous delivery of AAV8-SauCas9-sgRNA resulted in
340 accumulation of cytotoxic T-cells in the liver and subsequent removal of edited hepatocytes[12].
341 Therefore, the host immune response to Cas9-AAV in mice with pre-existing immunity would likely
342 look different than what we observed in naïve mice. In the Cas9-RNP group, we found that pre-
343 exposing mice to SpyCas9 protein with AddaVax™ adjuvant 4 weeks prior to stereotaxic surgery
344 synergistically increased systemic adaptive immune responses but did not result in any
345 deleterious phenotypes in our small cohort. Further studies are needed to assess the immune
346 response to Cas9-AAV and RNP in models with pre-existing immunity, but how well these
347 immunized mouse models recapitulate pre-existing immunity in humans is not clear. Furthermore,
348 breakdown of the BBB in the context of neurodegenerative disease or strong expression of the
349 tdTomato fluorescent reporter could also impact the host immune response[47,48].

350 In this study, we used a strong CMV-promoter to drive expression of SauCas9 from the
351 AAV, which allowed us to assess all subsets of edited cells in the striatum. Although the SauCas9
352 transgene was still expressed 4-months post-delivery, editing at predicted off-target sites was not
353 detected. Further work to experimentally determine guide-specific off-target sites, such as Guide-

Seq[49] or Circle-Seq[50], was not performed. To prevent potential genotoxic side-effects due to long-term Cas9 expression, we recommend applying additional safeguards, such as AAV self-inactivation strategies and cell-specific promoters[51–53]. While self-inactivating AAVs may improve safety, they may not be sufficient to reduce partial integration of the viral genome at the Cas9 cut site, which has been reported[36–39]. Strategies to mitigate the host response to genome editors include providing immunosuppressants with CRISPR-Cas9 infusion and screening for pre-existing immunity prior to dosing when translating *in vivo* editing to humans[54].

In conclusion, the cell penetrant 4x-Cas9-2x NLS fusion protein enables simple and effective delivery of Cas9 RNPs into neurons *in vitro* and *in vivo*. Our study is the first to comprehensively profile the host immune response to Cas9 in the brain, benchmark an RNP delivery strategy against the gold-standard for gene delivery in the CNS, and demonstrate feasibility of large-scale manufacturing. Given that Cas9-RNPs excel at editing high levels of neurons within a localized region of the brain, this is a promising modality to characterize therapeutic benefit in disease models in the future.

Materials & Methods

Plasmid construction

Cloning of several spacers into a plasmid encoding SauCas9 was performed as previously described. Oligonucleotides encoding sgRNAs were custom synthesized (Integrated DNA Technologies; IDT, Coralville, IA) and phosphorylated by T4 polynucleotide kinase (New England Biolabs; NEB, Ipswich, MA) for 30 min at 37°C. Oligonucleotides were annealed for 5 min at 95°C, cooled to room temperature and ligated into the BsmBI restriction sites of pSTX8,pKLT7.1_SaCas9prot_SaCas9guide plasmid. The following 23nt spacer sequences were cloned into the plasmid (spo 1: TGGTATGGCTGATTATGATCCTC; spo2: TCCCCCTGAACCTGAAACATAAA; spo3: GATGAGTTTGGACAAACCACAAC; spo4: TCCAGACATGATAAGATACATTG; spo5: CTCATCAATGTATCTTATCATGT), and plasmids were used for editing in mouse neural precursor cells *in vitro*. The best performing SauCas9 spacer (spo4: TCCAGACATGATAAGATACATTG) was then cloned into an AAV2 backbone plasmid. pX601-AAV-CMV::NLS-SaCas9-NLS-3xHA-bGHpA;U6::BsaI-sgRNA was a gift from Feng Zhang (Addgene plasmid # 61591 ; http://n2t.net/addgene:61591 ; RRID:Addgene_61591). Briefly, the plasmid was digested using BbsI and a pair of annealed oligos were cloned into the guide RNA destination site by Golden Gate assembly. Correct construction of all plasmids was verified by Sanger sequencing (UC Berkeley DNA Sequencing Facility).

Recombinant adeno-associated virus (AAV) Production

The custom AAV9-CMV-61591-HA-Bgh vectors were produced at Virovek (Hayward, CA) in insect Sf9 cells by dual infection with rBV-inCap9-inRep-hr2 and rBV-CMV-61591-HA-Bgh. The AAV9-CMV-GFP vectors were produced by dual infection with rBVinCap9-inRep-hr2 and rBV-CMV-GFP. The vectors were purified through two rounds of cesium chloride (CsCl) ultracentrifugation. The CsCl was removed through buffer exchange with two PD-10 desalting

394 columns. Viral titer (approximately 2e13 vg/mL) and purity were confirmed by nanodrop
395 spectrophotometer, real-time PCR, and SDS-PAGE protein gel analysis. The vectors were
396 passed through 0.2um sterilized filters, tested for endotoxins (< 0.6 EU/mL), as well as baculovirus
397 and Sf9 DNA contamination (not detected).
398
399 *Purification of low-endotoxin proteins in a laboratory setting*
400 Protein expression and purification was performed in the QB3 Macrolab at UC Berkeley
401 using a custom low-endotoxin workflow. Briefly, the plasmid, 4xNLS-pMJ915v2 (Addgene plasmid
402 # 88917; http://n2t.net/addgene:88917; RRID:Addgene_88917), was transformed into *E. coli*
403 Rosetta2(DE3)pLysS cells (Novagen) and an overnight culture was used to inoculate 1 L flasks
404 (12-24 L total per batch). Cells were grown for approximately 3 hours at 37°C then cooled to
405 16°C. At OD 0.8-0.9, cells were induced and harvested after 16-18 hours growth. Cells were lysed
406 by homogenization in a buffer containing 1mM $MgCl_2$ and benzonase (1:1000) to help reduce
407 viscosity and centrifuged to remove insoluble material. Purification by Ni affinity (10 mL Ni resin
408 for every 6 L cell lysate) was performed, and the bound protein was washed with 10 column
409 volumes of buffer containing 0.1% Triton-X114 at 4°C to help reduce endotoxins. Tag removal
410 with TEV protease (1:100) was performed overnight at 4°C, then heparin affinity was used to
411 concentrate each batch of protein which was then flash frozen and stored at -80°C. A Sephacryl
412 S300 size-exclusion column (SEC) and flow path were sanitized with 0.5 M NaOH overnight, then
413 washed with up to 3 column volumes of buffer to rinse and equilibrate the system. Frozen samples
414 were thawed, combined, and adjusted to 4.5 mL, and the S300 standard protocol was performed
415 for size-exclusion. Samples were refrigerated overnight, and sanitation and size-exclusion were
416 repeated the next day to further reduce endotoxin contamination. Peak fractions were pooled,
417 concentrated to 40μM, aliquoted at 50μL, flash frozen in liquid nitrogen, and stored at -80°C in
418 sterile, endotoxin-free Buffer 1 (25 mM NaP (pH 7.25), 300 mM NaCl, 200 mM trehalose (Sigma
419 Aldrich #T5251, St. Louis, MO)). Final average protein yield was 1 mg per 1 L cells. Plasmids for

2xNLS-SauCas9-2xNLS, 3xNLS-SauCas9-2xNLS, and 4xNLS-SauCas9-2xNLS were created by deletion mutagenesis using the existing 4xNLS construct as a template. The genes were fully sequenced to confirm no additional mutations were introduced during the mutagenesis procedure.

Purification of ultra-low endotoxin proteins in an industrial setting

4x-SpyCas9-2x NLS protein was manufactured according to Aldevron proprietary workflows for expression and purification of gene editing nucleases. Briefly, the gene for 4x-SpyCas9-2x NLS was synthesized (ATUM Bio, Sunnyvale, CA) and cloned into a pD881 expression vector (ATUM). Expression-ready plasmid DNA was transformed into E. coli BL21(DE3) (New England Biolabs) culture in animal-free TB media. At the appropriate OD600, expression was induced with 2.0% (w/v) Rhamnose and growth culture was harvested by centrifugation. Cells were lysed via dual-pass high-pressure homogenization and clarified via centrifugation. The clarified lysate was purified via multi-step chromatography using standard/commercially available resins. In the final chromatography step, the product is eluted via step elution and pooled to maximize final protein purity and minimize endotoxin. Product was dialyzed into the final formulation buffer, underwent three (3) exchanges of buffer, and was pooled into a sterile vessel for final filtration and dispensing. Product was evaluated for key quality attributes including endotoxin via PTS Endosafe assay (Charles River Labs, Cambridge, MA).

Quantification of endotoxins in Cas9 RNPs

Proteins, guide RNAs, and pre-formed RNP complexes were subjected to several assays to quantify endotoxin burden according to the manufacturer's instructions. All assays were performed with autoclaved or certified pyrogen-free plasticware and endotoxin (ET)-free water. The plate-reader based LAL assay was performed with the Endosafe Endochrome-K kit (Charles River, #R1708K), where a control standard endotoxin (CSE) was diluted from 5 EU/mL to 0.005 EU/mL. Samples were diluted 1:100 and plated in triplicate. An equal volume of LAL was added

446 to each well. A Tecan Spark plate reader (Tecan, #30086376, Mànnendorf, Switzerland) with
447 SparkControl magellan V 2.2 software was used at 37°C to read absorbance at 405nm every 30
448 seconds for 100 cycles. Time at which absorbance crossed optical density (OD) of 0.1 was
449 recorded and used to determine endotoxin levels.

450 The cartridge-based LAL assay was performed using an Endosafe nexgen-PTS machine with
451 R&D cartridges as recommended (Charles River, cat # PTS2005, 0.05 EU/mL sensitivity). Briefly,
452 samples were diluted 1:50 in a large volume of ET-free water, vortexed, and 25µL was loaded
453 into each of the four lanes of the cartridge, where two lanes contain CSE spike-in to calculate
454 efficiency of the assay, which is valid from 50%-200% recovery. The final valid ET value was
455 recorded from the duplicate measurement from a single cartridge.

456 The PyroGene Recombinant Factor C Endpoint Fluorescent Assay (Lonza, Walkersville, MD,
457 cat # 50-658U) was performed as recommended. Kit-supplied CSE was diluted from 5 EU/mL to
458 0.005 EU/mL and samples were diluted 1:100 in ET-free water and added to a plate in triplicate.
459 The plate was heated at 37°C for 10 minutes, then an equal volume of working reagent was added
460 to each well. Fluorescence was read immediately at time 0 and again after incubating for 60
461 minutes. Relative fluorescence units (RFUs) of the ET-free water only blank wells were subtracted
462 from all measurements, then delta RFUs between the two time points was calculated, and a linear
463 regression was applied to the standard curve to calculate EUs in the samples. Fluorescence
464 measurements were performed on a Cytation5 with Gen 5 3.04 software (BioTek, Winooski, VT).

465 HEK-Blue cells (hTLR4 and Null2) were purchased from Invivogen (San Diego, CA) and were
466 grown under BSL2 conditions (37°C with 5% CO_2) to measure SEAP production downstream of
467 NFkappaB activation following treatment with Cas9 proteins, guide RNAs, and RNPs *in vitro* as
468 recommended. Cells were grown in T-75 flasks with supplied antibiotic selection markers and
469 passaged at 70% confluency. Cells were detached with gentle scraping in 1x PBS, centrifuged,
470 counted, and plated for experiments in freshly prepared HEK-Blue Detection Media at
471 approximately 32,000 cells per well in a 96-well plate. 180µL of cell suspension was plated directly

472 into 20μL of diluted CSE (5 to 0.078 ng) or samples (diluted to 10μM) and incubated overnight at
473 37°C. Absorbance was read at 620nm in a Tecan Spark plate reader (Tecan, #30086376,
474 Mànnendorf, Switzerland).
475
476 *Neural progenitor cell (NPC) line creation and culture*
477 Neural progenitor cells were isolated from Ai9-tdTomato homozygous mouse embryos
478 (day 13.5) by microdissection of cortical tissues into Hibernate E (#HECA, Brain Bits, LLC,
479 Springfield, IL) and processing with the Neural Dissociation Kit with papain (#130-092-628,
480 Miltenyi, Bergisch Gladbach, Germany) according to the manufacturer's instruction. Single cells
481 grew into non-adherent neurospheres, which were maintained in culture media (DMEM/F12
482 (ThermoFisher #10565-018, Waltham, MA), B-27 supplement (#12587-010), N-2 supplement
483 (#17502-048), MEM non-essential amino acids (#11140-050), 10 mM HEPES (#15630-080),
484 1000X 2-mercaptoethanol (#21985-023), 100X Pen/Strep (#15140-122)) supplemented with
485 growth factors (FGF-basic (Biolegend #579606) and EGF (ThermoFisher #PHG0311) to a final
486 concentration of 20 ng/mL in media. Neurospheres were passaged every six days using the
487 Neural Dissociation Kit to approximately 1.5 million cells per 10-cm dish and growth factors were
488 refreshed every 3 days. Cells were authenticated by immunofluorescent staining for Nestin and
489 GFAP, routinely tested for mycoplasma, and were used for experiments between passages 2 and
490 20. Dissociated cells were grown in monolayers in 96-well plates pre-coated with poly-DL-
491 ornithine (SigmaAldrich, #P8638), laminin (SigmaAldrich #11243217001) and fibronectin
492 (SigmaAldrich #F4759) at 10,000-30,000 cells per well for direct delivery and nucleofection
493 experiments.
494
495 *Human induced pluripotent stem cell differentiation into NPCs and culture*
496 MSC-iPSC1 cells were a generous gift from Boston Children's Hospital. iPSCs were
497 differentiated into NPCs based on dual SMAD inhibition as previously described. Briefly, iPSCs

were plated onto Matrigel in the presence of 10μM Y-27632 (Sigma #Y0503) at a density of 200,000 cells/cm^2. The next day (day 0) media was changed to KSR media (Knockout DMEM (ThermoFisher #10829018), 15% Knockout serum replacement (ThermoFisher #10828010), L-glutamine (1mM), 1% MEM Non-essential amino acids, and 0.1mM B-mercaptoethanol). Media was changed daily during differentiation and gradually changed from KSR media to N2/B27 media (Neurobasal medium (ThermoFisher #21103049), GlutaMAX Supplement (ThermoFisher #35050061), N-2 supplement (ThermoFisher #17502048) and B-27 supplement (ThermoFisher #17504044)) by increasing N2/B27 media to 1/3 on day 4, 2/3 on day 6 and full N2/B27 media on day 8. For the first 12 days of differentiation media was supplemented with 100nM LDN193189 (Sigma #SML0559) and 10μM SB431542 (Tocris Bioscience #1614, Bristol, England). For the first 4 days media was also supplemented with 2μM XAV939 (Tocris Bioscience #3748). On day 19, NPCs were dissociated with StemPro Accutase (ThermoFisher #A1110501) and replated onto Matrigel for expansion. NPCs were passaged every 6 days and maintained in NPC media (DMEM/F12, N2 supplement, B27 supplement and 20ng/ml bFGF (Corning, #354060, Corning, NY)) with media changes every other day. For direct delivery experiments, 12,000 cells were seeded in Matrigel in a 96-well plate and treated in triplicate with 100pmol of 4xNLS-SpyCas9-2xNLS RNPs with the EMX1 guide RNA (spacer: 5' GAGTCCGAGCAGAAGAAGAA) or non-targeting guide RNA (spacer: 5' AACGACTAGTTAGGCGTGTA). In the Lipofectamine™ CRISPRmax group (ThermoFisher, #CMAX00003), 3μg of 0xNLS-SpyCas9-2xNLS protein (18 pmol) was mixed with sgRNA (1:1 molar ratio) in 8μL OptiMEM with 6μL of Cas9 Plus Reagent (1 μg protein: 2μL reagent) and was mixed with a second tube containing 3.6μL CRISPRmax reagent in 8μL OptiMEM, incubated for at least 5 minutes and was immediately distributed to cells in triplicate (1μg RNP per well), according to the manufacturer's recommendations.

Cas9 ribonucleoprotein (RNP) assembly and delivery to cells

For cell culture experiments, RNPs were prepared immediately before use at a 1.2:1 molar ratio of single guide RNA (Synthego, Redwood City, CA) to protein (QB3 Macrolab or Aldevron). The solution was incubated for 5-10 minutes at room temperature. For nucleofection, RNPs were formed at 10μM in 10μL of pre-supplemented buffer (Lonza P3 Primary Cell 96-well Kit, #V4SP-3096). A 15μL suspension of 250,000 mouse NPCs was mixed with 10μL RNP solution and added to the nucleofection cuvette. Nucleofection was performed using the 4D Nucleofector X Unit (Lonza, #AAF-1003X) with pulse code EH-100 and cells were recovered with 75 μL media per well approximately 2 minutes post-nucleofection. Nucleofected cells were then transferred to 100 μL fresh media in 96-well plates in triplicate and allowed to grow for 5 days at 37°C before analysis by flow cytometry for tdTomato expression. For direct delivery, RNPs were formed at 10μM in 10μL of sterile Buffer 1 (25 mM sodium phosphate pH (7.25), 100 mM NaCl, 200 mM trehalose). After NPCs were grown for two days in an adherent monolayer, 10μL was added to cell monolayer ("direct delivery") for a final concentration of 1μM (100pmol RNP/100μL media). Media was changed 48-hours post-treatment and cells were collected 5 days post-treatment for analysis by flow cytometry for tdTomato expression or 4 days post-treatment for DNA sequencing. For *in vivo* experiments, RNPs were prepared similarly at 10μM concentration in Buffer 1 and were incubated at 37°C for 10 minutes. RNPs were sterile filtered by centrifuging through 0.22μm Spin-X cellulose acetate membranes (Corning CoStar, #32119210) at 15,000xg for 1 minute at 4°C. RNPs were then concentrated using 100kDa Ultra-0.5 ml Centrifugal Filter Unit (Amicon, #, Burlington, MA) at 14,000xg at 4°C until the final desired concentration was reached (25-100μM, minimum 50μL volume) and collected by centrifuging at 1,000xg for 2 minutes. RNPs were then divided into single-use 20μL aliquots, flash frozen in liquid nitrogen, and stored at -80°C until the experiment. Prior to intracranial injection, RNPs were thawed, pipetted to mix, loaded into a 25μL syringe (Hamilton, #7654-01, Reno, NV) and injected with custom 29-gauge CED cannulas.

AAV9 transduction

A single 50µL aliquot of AAV9-CMV-SauCas9-U6-sgRNA or AAV9-CMV-GFP (Virovek) was thawed from -80°C and stored at 4°C. AAV9 was diluted in 1x PBS without calcium or magnesium to the desired concentration. For *in vivo* experiments, AAV was diluted on the day of surgeries to 3e9 vg/µL and stored on ice until loaded into the syringe. 5µL was injected in each hemisphere to a final dose of 1.5e10 vg per hemisphere using the CED. For cell culture experiments, serial dilutions were performed from 1.6e9 vg/µL to 2e8 vg/µL (lowest MOI = 200,000) and 10µL of each were added into 96-well plates in triplicate and maintained for 3 days or 9 days prior to flow cytometry for GFP expression (transduction) and tdTomato expression (genome editing). AAV9 was added at the same time as NPC seeding for optimal transduction.

Empty capsid quantification by cryo-electron microscopy

AAV samples were frozen using FEI Vitrobot Mark IV cooled down to 8°C at 100% humidity. Briefly, 4 µl of AAV9 capsids containing GFP or Cas9 cargo was deposited on 2/2 400 mesh C-flat grids (Electron Microscopy Sciences, Hatfield, PA, #CF224C-50), which were previously glow discharged at 15 mA for 15 s on PELCO easyGLOW instrument. Grids were blotted for 3 s with blot force 8 and wait time 2.5 s. Micrographs were collected manually on Talos Arctica operated at 200 kV and magnification 36,000x (pixel size 1.14 Å/pix) using a super-resolution camera setting (0.57 Å/pix) on K3 Direct Electron Detector. Micrographs were collected using SerialEM v. 3.8.7 software. Capids were counted manually by three blinded reviewers for each image and the three counts were averaged and reported as percentage empty capsids between the two groups.

Analysis of editing in vitro

tdTomato positivity was assessed by flow cytometry using IGI facilities on the Attune NxT (Thermo Fisher, AFC2). Briefly, mouse NPCs were washed once with 1x PBS, harvested with

0.25% trypsin, neutralized with DMEM containing 10% FBS, and resuspended in 150uL of 1x PBS per well of a round-bottom 96-well plate for analysis. The percentage of tdTomato$^+$ cells from each well was recorded. For analysis of genomic DNA (gDNA), media was removed, cells were rinsed once with 1X PBS, then incubated with 100 µL QuickExtract solution (Lucigen CorporationSupplier Diversity Partner QuickExtract DNA Extraction Solution 1.0, Fisher, #QE09050) at 37°C for 5 minutes. The cell lysate was then moved to a thermal cycler and incubated at 65°C for 20 minutes and 95°C for 20 minutes. gDNA was used in PCR reactions to generate amplicons of approximately 150-300bp for Illumina sequencing. A list of primers used for NGS is provided in Supplementary Table 1. Sequencing was performed with Illumina MiSeq in the IGI Center for Translational Genomics and reads were analyzed in CRISPResso (website).

Stereotaxic infusion of Cas9 RNPs and AAVs

Ai9 mice (Jackson Laboratory, #007909, Bar Harbor, ME) were group housed at the University of California, Berkeley with a 12-hour light-dark cycle and allowed to feed and drink *ad libitum.* Housing, maintenance, and experimentation of the mice were carried out with strict adherence to ethical regulations set forth by the Animal Care and Use Committee (ACUC) at the University of California, Berkeley. Cas9-RNP and AAVs were prepared on-site at the University of California, Berkeley for injection into male and female tdTomato Ai9 mice between 2 to 5 months of age. All tools were autoclaved and injected materials were sterile. Mice anesthetized with 2% isoflurane, given pre-emptive analgesics, and were arranged on Angle-two stereotactic frame (Leica, Nussloch, Germany). The incision area was swabbed with three alternating wipes of 70% ethanol and betadine scrub with sterile applicators prior to performing minimally damaging craniotomies. The stereotaxic surgery coordinates used for targeting the striatum, relative to bregma, were +0.74 mm anterioposterior, ±1.90 mm mediolateral, −3.37 mm dorsoventral. Bilateral infusion of Cas9 RNPs (5µL at 10µM to 100µM) or Cas9 AAVs (5µL at 3e9 vg/µL) was performed with a syringe pump to deliver 0.5 µL per minute (Model 310 Plus, KD Scientific,

Holliston, MA). For intracerebroventricular (ICV) infusion of Cas9 RNPs, cannulas were placed at –0.7 mm posterior, +/−1.2 mm lateral, and –2.5 mm according to Paxinos atlas of the adult mouse. Post-infusion, the syringes were left in position for 2 minutes before slow removal from the injection site, which was then cleaned, sutured, and surgically glued. Throughout the procedure, mice were kept at 37°C for warmth and Puralube Vet Ointment (Dechra, NDC #17033-211-38, Northwich, England) was applied to the outside of the eyes. For ICV injection of p0 neonatal mice, anesthesia was induced by hypothermia then 4µL of 100µM Cas9-RNP was injected with a hand-held 33-gauge needle unilaterally with 10% Fast Green dye to visualize distribution from one ventricle throughout the CNS. The needle was inserted 2 mm deep at a location approximately 0.25 mm lateral to the sagittal suture and 0.50-0.75 mm rostral to the neonatal coronal suture. RNP was slowly injected, then the needle was held in place for 15 seconds, and mice were monitored until recovery. For intrathecal injection, anesthetized mice received a 5, 25, or 50 µL bolus injection of Cas9 RNP at 300µM. The 29-gauge needle was inserted at the L6-S1 vertebral junction and angled slightly rostrally for the injection. Mice were allowed to fully recover before being transferred back to their housing. Recovery weight following all procedures was monitored daily for one week and mice were housed without further disruption for various time periods until tissue collection.

Tissue collection and immunostaining

At the defined study endpoints (3, 21, and 90-days post-injection), mice were placed under anesthesia and tissues were perfused with 10mL of cold PBS and 5mL of 4% paraformaldehyde (PFA, Electron Microscopy Sciences, #15710, Hatfield, PA). Brains were post-fixed overnight in 4% PFA at 4°C, rinsed 3x with PBS, then cryoprotected in a 10% sucrose in PBS solution for approximately 3 days. Brains were embedded in optimal cutting temperature (OCT, Thermo Fisher, #23-730-571) media, and stored at -80°C. Brains were cut at 20-35 µm-thick sections using a cryostat (Leica CM3050S) and transferred to positively charged microscope slides. For

immunohistochemical analysis, tissues were blocked with solution (0.3% TritonX-100, 1% bovine serum albumin (SigmaAldrich #A9418), 5% normal goat serum (SigmaAldrich, #G9023)) before 4°C incubation overnight with primary antibody in blocking solution. The next day, tissues were washed three times with PBS and incubated with secondary antibodies for one hour at room temperature. After three PBS washes, samples were incubated with DAPI solution (0.5 ug/mL, Roche LifeScience, Penzberg, Germany) as a DNA fluorescence probe for 10 minutes, washed three times with PBS, submerged once in deionized water, and mounted with glass coverslips in Fluoromount-G slide mounting medium (SouthernBiotech, Birmingham, AL). Primary antibodies included rabbit polyclonal anti-S100β (1:500, Abcam, #ab41548, Cambridge, England), rabbit polyclonal anti-Olig-2 (1:250, Millipore Sigma, #AB9610, Burlington, MA), rabbit polyclonal anti-doublecortin (1:800, Cell Signaling Technology, #4604, Danvers, MA), rabbit polyclonal anti-Ki67 (1:100, Abcam, #ab15580), mouse monoclonal anti-NeuN (1:500, Millipore Sigma, #MAB377), rabbit polyclonal anti-DARPP-32 (1:100, Cell Signaling Technology, #2302), rabbit polyclonal anti-Iba1 (1:100, Wako Chemicals, #019-19741, Richmond, VA), mouse monoclonal anti-glial fibrillary acidic protein (1:1000, Millipore Sigma, #MAB3402), rat monoclonal anti-CD45 (1:200, Thermo Fisher, #RA3-6B2), and rabbit polyclonal anti-CD3 (1:150, Abcam, #ab5690). Secondary antibodies included donkey anti-rat 488 (1:500, Thermo Fisher, #A-21208), goat anti-rabbit 488 (1:500, Thermo Fisher, #A32731), goat anti-rabbit 647 (1:500, Thermo Fisher, #A21245), and goat anti-mouse IgG1 647 (1:500, Thermo Fisher, #A-21240).

Fluorescent imaging and image quantification

Whole brain sections were imaged and stitched using the automated AxioScanZ1 (Zeiss, Oberkochen, Germany) with a 20x objective in the DAPI and tdTomato channels. Images generated from slide scanning were viewed in ZenLite software as CZI files. Images were then exported to ImageJ, Imaris, or QuPath for further quantification. The area of reflux from CED and blunt needles was calculated directly in ZenLite using the shape and area analysis tools.

Immunostained cells and tissues were imaged on the Evos Revolve widefield microscope using a 20x objective or Stellaris 5 confocal microscope (Leica) with a 10x or 25x water-immersion objective to capture data in DAPI, FITC, tdTomato and CY5 channels. Approximately four images were taken at 20-25x per hemisphere across multiple sections for image quantification of CD45, Iba1, and CD3 (8-12 images quantified and averaged per injection). Approximately four to six z-stack images were captured and stitched per hemisphere for qualitative images of Iba1 and for quantification of NeuN, DARPP-32, ALDH1L1, and OLIG2 with tdTomato at 1024x1024 pixel resolution with a scanning speed of 100-200.

Measurements of striatal editing by volume were conducted using QuPath software (version 0.3.2) from images obtained from the Zeiss AxioscanZ1. Briefly, regions of interest (ROIs) were drawn to outline the border of each striatum and the inner area of tdTomato editing using the polygon tool to create annotations. All coronal plane areas were automatically calculated. Dorsoventral coordinates (relative to bregma) were then estimated in millimeters by consulting the Mouse Brain Atlas (C57BL/6J Coronal). Approximate tissue volume was calculated by averaging outlined areas between consecutive sections to represent the mean area across a dorsoventral segment and multiplying by the difference in dorsoventral coordinates. Edited striatal volumes were then divided by total striatal volumes to obtain percent editing. Additional tdTomato^{+} cell count measurements were conducted in Imaris software version 10.0 (Oxford Instruments, Abingdon, UK). Briefly, ROIs were drawn over each hemisphere (including cells in all brain sub-structures) using the “Segment only a Region of Interest” tool, and positive cells detected using the automated “Spots” tool to provide cell counts. Positivity thresholds were adjusted for each image to accurately capture edited cells manually. Counts of tdTomato cells on each image were then related back to approximate coordinates relative to bregma using the Mouse Brain Atlas (C57BL/6J Coronal) to quantify the distribution of edited cells.

Cell type specific measurements were conducted using QuPath software (version 0.3.2) on images obtained from Stellaris 5 z-stack maximal projections. ROIs were again drawn around

678 areas of observed tdTomato editing, using the polygon tool to create a single annotation per
679 image. Cell count calculations were performed using the “Cell Detection” and “Positive Cell
680 Detection” tools, adjusting “Cell Mean” thresholds accordingly for each channel and image.
681 Percent area and intensity measurements were performed in Fiji/ImageJ software (version
682 2.1.0/1.53c). Images were converted to 32-bit, and thresholds were adjusted to detect the
683 corresponding stained area. Measurements were set to include area, minimum, maximum, and
684 mean gray value, and area fraction, as well as to limit to threshold. All image quantification was
685 performed on 2-5 serial sections with 3-10 independent injections per group for each analysis.
686 Cell counts, area, intensity, and volume measurements were in general averaged from serial
687 sections and were then grouped with other biological replicates, including independent injections,
688 to report the treatment group average with standard deviation displayed by bar graph or box and
689 whisker plot.
690
691 *Serum collection and ELISA*
692 Blood was collected from mice at the time of euthanasia, allowed to clot at room temperature
693 for 15-30 minutes, then centrifuged for 5 minutes at 2,000xg. Sera was collected and placed
694 immediately on dry ice then stored at -80°C. Enzyme-linked immunosorbent assays were
695 performed using the SeraCare Protein Detector™ HRP Microwell Anti-Mouse ELISA Kit, #5110-
696 0011 (54-62-18) according to the manufacturer’s recommendations. First, 96-well plates were
697 coated with antigens of interest (0.5 µg protein per well for SauCas9 and SpyCas9 (4xNLS protein
698 variants) and approximately 1e9 empty AAV capsids per well) overnight at 4°C. Wells were
699 washed three times and blocked at room temperature for one hour. Serum samples were then
700 incubated in wells at varying concentrations (1:50 to 1:10,000 dilution) in 1X blocking buffer for
701 four hours at room temperature, along with monoclonal antibody controls to generate a standard
702 curve. Standards included CRISPR/Cas9 Monoclonal Antibody 7A9 (Epigentek, #A-9000-050,
703 Farmingdale, NY), GenCRISPR™ SaCas9 Antibody 26H10 (GenScript, #A01952, Piscataway,

704 NJ), and Anti-Adeno-associated Virus 9 Antibody clone HL2374 (Millipore Sigma, #MABF2326-
705 25UG). Following three additional washes, the HRP secondary antibody was added at 1:500 in
706 1x blocking buffer and incubated for one hour. Wells were then washed three more times, and
707 peroxidase substrate solutions were added. Absorbance was recorded at a wavelength of 405nm
708 with Cytation5 plate reader with Gen 5 3.04 software (BioTek). Serum antibody concentrations
709 were calculated using five-parameter logistic curve (5PL) data analysis at MyAssays.com and
710 normalized to sham controls.
711
712 *Splenocyte collection and enzyme linked immunospot (ELISpot)*
713 Spleens were collected at the time of euthanasia and stored in media composed of RPMI
714 1640 (ThermoFisher, #11875-119) with 10% FBS (VWR, #89510-186, Radnor, PA) and 1% P/S
715 (ThermoFisher, #15140-122). Briefly, spleens were physically dissociated by forcing through a
716 100µm cell strainer in 10mL of media then single cells were passed through a 70µm strainer and
717 centrifuged at 200xg for 5 minutes. Cells were resuspended in 5mL of 1x RBC Lysis Buffer
718 (Miltenyi # 130-094-183) for approximately 3 minutes, then centrifuged again and resuspended in
719 media for counting. The mouse interferon-gamma (IFN-γ) ELISpot kit (R&D Systems, #EL485,
720 Minneapolis, MN) was used according to the manufacturer's instructions to assess activation of
721 splenocytes, containing T-cells, in response to treatment with Cas9 proteins. Briefly, the plate was
722 pre-washed and 200µL of media for at least 20 minutes in the incubator, prior to adding cells at
723 300,000 per well in 100µL media. Treatments at 2x dose were prepared in media and 100µL was
724 added to wells in triplicate (final 5 µg/mL concentration). Plates were wrapped in foil and incubated
725 for 48 hours without disturbing. Concanavalin A (SigmaAldrich, #C5275) was used as a positive
726 control for cell mediated IFN-γ production (final 4 µg/mL concentration). After 48-hours, cells were
727 removed and the secreted analyte was detected with immunostaining using the kit-provided
728 biotinylated monoclonal antibody specific for mouse IFN-γ, streptavidin-conjugated alkaline

729 phosphatase, and stabilized detection mixture of 5-Bromo-4-Chloro-3'Indolylphosphate-p-
730 Toluidine Salt (BCIP) and Nitro Blue Tetrazolium Chloride (NBT). After staining, plates were dried
731 overnight and spot forming units were imaged and counted on the ImmunoSpot S6 Macro
732 Analyzer (Cellular Technology Limited, Shaker Heights, OH).
733
734 *Immunization of mice to Cas9 with adjuvant*
735 AddaVax™ (Invivogen, vac-adx-10), a squalene-based oil-in-water nano-emulsion, was
736 mixed with an equal volume containing 25µg of 4x-SpyCas9-2x protein diluted in sterile buffer at
737 room temperature for a final injection volume of 50µL. Mice received two 25µL subcutaneous
738 injections of the AddaVax:Cas9 mixture (immunized) or AddaVax:Buffer alone (sham) with a 30-
739 gauge insulin syringe into each flank. After four weeks, stereotaxic surgery with bilateral injections
740 of 5µL of 25µM Cas9-RNPs was performed in a subset of mice. Mice showed no signs of pain or
741 distress following treatment with AddaVax and no acute events were noted after surgery. Mice
742 that received AddaVax, with or without surgery, were euthanized 6-weeks post-subcutaneous
743 injections. Brains, serum, and spleens were collected for analysis of adaptive immune responses
744 against repeated exposure to Cas9.
745
746 *DNA/RNA extraction from brain tissue slices and quantitative RT-PCR, droplet digital PCR, and*
747 *long-read sequencing*
748 Brains were collected at 3, 14, and 28-days or 4-months for DNA and RNA analysis.
749 Briefly, mice were placed under anesthesia and perfused with cold PBS. Brains were harvested
750 and cut into 2-mm sections using a matrix around the injection site (Zivic Instruments, Pittsburgh,
751 PA). The slices were transferred onto chilled glass slides and further trimmed to approximate
752 30mg tissue weight (1–1.25 mm wide × 2 mm long). Tissues were flash frozen in liquid nitrogen
753 then stored at -80°C until processing. DNA and RNA were collected from tissues using the AllPrep
754 DNA/RNA Mini Kit (Qiagen, #80204, Venlo, Netherlands) according to the manufacturer's

755 instructions. Briefly, brains were homogenized in 1.5 mL tubes with a disposable pestle directly in
756 RLT lysis buffer supplemented with 2-mercaptoethanol, then passed through Qiashredder
757 columns to further homogenize prior to adding directly to the DNA and RNA binding columns.
758 DNA was eluted in 100µL of EB, and RNA was eluted in 40 µL RNAse-free water. Concentrations
759 of nucleic acids were measured by nanodrop spectrophotometer and samples were stored at -
760 20°C.

761 Gene expression was quantified across multiple samples using a Custom RT^2 PCR Array
762 (Qiagen, #330171, CLAM45824) and analyzed using the RT^2 Profiler PCR Data Analysis Tool on
763 GeneGlobe (Qiagen). For reverse transcription, the RT^2 First Strand Kit (Qiagen, #330404) was
764 used according to the manufacturer's instructions. cDNA was diluted in water and added to the
765 RT^2 SYBR Green qPCR Mastermix (Qiagen, #330502) then distributed across the 24-wells
766 containing verified assay primers and controls (PCR array reproducibility control, reverse
767 transcription efficiency control, genomic DNA contamination control, two house-keeping genes,
768 and 19 experimental genes). Quantitative real-time PCR was performed on the CFX96 Touch
769 Real-Time PCR System (BioRad). cDNA was also used in a droplet digital PCR reaction to
770 measure SauCas9 expression at the 4-month time-point. qPCR assay IDs are included in Tables
771 S1 and S2.

772 DNA was also used for PCR amplicon sequencing of predicted off-target sites and for
773 droplet digital PCR (ddPCR). Off-target sites were predicted using Cas-OFFinder
774 (http://www.rgenome.net/cas-offinder/)[55]. Predicted off-targets are described further in Tables S3
775 and S4. Primers were designed using NCBI Primer Blast with an amplicon size of 250-300bp,
776 listed in Table S1. Sequencing was performed with Illumina MiSeq in the IGI Center for
777 Translational Genomics and reads were analyzed in CRISPResso2
778 (http://crispresso.pinellolab.org)[56].

779 For droplet digital PCR (ddPCR), a custom NHEJ ddPCR assays were generated using
780 the online Bio-Rad design tool (Table S2). Assays for SauCas9 and SpyCas9 contain both the

781 primers and probes (HEX-probe spanning the cut-site and a distal reference FAM-probe). To
782 prepare the reactions, 110 ng of gDNA was combined with the 20x assay, 2x ddPCR Supermix
783 for Probes (No dUTP), 1µL of of SmaI restriction enzyme (2 units per reaction), and water up to
784 22µL. Then 20 µl of each reaction mix was added to DG8TM Cartridges (Bio-Rad #1864008,
785 Hercules, CA) followed by 70 µl of Droplet Generation Oil for Probes (Bio-Rad #1863005) and
786 droplets were formed in the QX200 Droplet Generator. Droplets were then transferred to a 96-
787 well plate and thermal cycled according to the manufacturer's recommendation with a 3-minute
788 annealing/extension step. After thermal cycling, the sealed plate was placed in the QX200 Droplet
789 Reader and data was acquired and analyzed in the QuantaSoft Analysis Pro Software using the
790 "Drop-Off" analysis, manually setting the thresholds for cluster calling (FAM+ only, FAM+ HEX+
791 cluster, FAM-HEX- cluster), and exporting fractional abundance calculations.

792 Long-read sequencing of the tdTomato locus was performed on DNA isolated from the
793 treated mouse brains. Briefly, PCR amplicons were generated on 16 samples from the 4-month
794 treatment groups using primers with unique barcodes for sample de-multiplexing. The KAPA HiFi
795 Hotstart PCR Kit (Roche, KK2502) was used to amplify the 1100 bp product and reactions were
796 cleaned with AMPure XP magnetic beads (Beckman Coulter Inc., Brea, CA) prior to analysis by
797 Qubit and Bioanalyzer with the DNA 7500 Kit (Agilent, #5067-1506, Santa Clara, CA). Samples
798 were combined and 1µg of pooled amplicons and submitted (> 20ng/µL) for sequencing with one
799 PacBio Sequel 8M SMRT Cell at the QB3 Vincent Coates Genomic Sequencing Lab, yielding
800 approximately 110,000 reads per sample. Data were analyzed using a custom pipeline to identify
801 viral fragment trapping during DNA repair. Briefly, PacBio circular consensus reads were trimmed
802 with Cutadapt (Version 4.1)[57], then aligned to the AAV vector using NGMLR (Version 0.2.7)[58] to
803 generate BAM files. Soft-clipped regions of aligned reads were extracted using PySam (Version
804 0.18.0, https://github.com/pysam-developers/pysam) to parse CIGAR strings, then realigned to
805 the tdTomato locus with NGMLR to verify integration within 200 bp of the cut site. Confirmed

integrations were visualized along the AAV genome using pyGenomeTracks (Version 3.3) and coverage statistics were summarized using PySam[59,60].

Statistical analyses

The data presented in bar graphs and box and whisker plots are averages across multiple technical and biological replicates and error bars represent the standard deviation. Sample sizes are indicated in the text and figure legends and generally refer to technical injection replicates (two technical replicates, i.e., bilateral injections, per one biological replicate). When comparing two groups with normal distribution, an unpaired student's t-test was performed in Prism 9 (GraphPad Software version 9.4.1). When comparing multiple groups, a one-way ANOVA with Tukey's multiple comparison test was performed in Prism 9 (GraphPad Software version 9.4.1). The RT-qPCR experiments used Student's t-test of the experimental group compared to the sham control (Qiagen GeneGlobe RT^2 Profiler PCR Data Analysis). $p \leq 0.05$ was considered significant

Data Availability Statement

Long-read sequencing (BAM files from PacBio circular consensus sequence, CCS) are available in Sequence Read Archive (SRA). Accession number: [#]. All additional data is available upon request.

Acknowledgements

Thank you to Netravathi Krishnappa and Christopher Hann-Soden for library preparation, sequencing, and analysis at the IGI Center for Translational Genomics and the QB3 Vincent J. Coates Genomics Sequencing Lab. Thank you to members of the Doudna lab at IGI, particularly Drs. Matthew Kan and Jennifer Hamilton, as well as Brett Staahl, Ross Wilson, and Fyodor Urnov for intellectual contributions and support. Thank you to Aldevron, LLC for collaboration on this

effort, especially Samantha Foti, Allison Pappas, David Yoder, and Max Sellman. Thank you to Denise Schichnes and Steven Ruzin at the CNR Berkeley Imaging Facility at the University of California, Berkeley as well as Feather Ives, Anita Flynn, and Holly Aaron at the CRL Microscopy Imaging Core (RRID:SCR_017852) at the University of California, Berkeley. Thank you to Eva Harris and lab members for the use of the ELISpot plate reader. Thank you to Kathy Snow and Ethan Saville at Jackson Laboratories for discussion about QuPath image quantification software. Thank you to Drs. Greg Barton and David Raulet for intellectual discussions regarding endotoxins and immune response. Thank you to Biogen Inc., especially Robin Kleinmen and Anirvan Ghosh, for funding and intellectual contributions. Thank you to Ruth L. Kirschstein F32 NIGMS for funding (E.C.S).

Author Contributions

E.C.S performed the experiments, analysis, and manuscript preparation and oversaw contributions from researchers (R.A., E. A., S.E.K., A.S., N.L., M.K.) who assisted with tissue processing, cloning, ELISAs, immunohistochemistry, and image analysis. E.C.S., J.K.S., and M.H.K. designed *in vivo* experiments, performed stereotaxic surgeries, confocal microscopy, and quantitative PCR. M.T. performed long-read NGS sequencing analysis. E.C.S. performed isolation and culture of mouse primary cells, flow cytometry, and ELISpot assays. K.S. performed electron microscopy. V.S.R. and L.T.V. performed human stem cell culture and differentiation. C.J., A.W., T.M., A.K., and T.F. performed custom low-endotoxin protein expression and purification. D.F.S. and J.A.D. approved the experiments, provided intellectual contributions, and co-wrote the manuscript.

Declaration of Interests Statement

J.A.D. is a cofounder of Caribou Biosciences, Editas Medicine, Scribe Therapeutics, Intellia Therapeutics and Mammoth Biosciences. J.A.D. is a scientific advisory board member of Vertex,

Caribou Biosciences, Intellia Therapeutics, eFFECTOR Therapeutics, Scribe Therapeutics, Mammoth Biosciences, Synthego, Algen Biotechnologies, Felix Biosciences, The Column Group and Inari. J.A.D. is a Director at Johnson & Johnson and Tempus and has research projects sponsored by Biogen, Pfizer, Apple Tree Partners and Roche. Patent applications have been filed relating to the technologies described herein. The indicated authors are employees of Aldevron, LLC, which offers proteins, pDNA, mRNA and reagents for sale similar to some of the compounds described in this manuscript.

Keywords (5-10)

CRISPR-Cas9, Genome Editing, Viral Vectors, Non-viral Delivery, Mouse, Brain, Host Immune Response, Neurons, Microglia, Endotoxin/LPS

References

1. Heidenreich, M. & Zhang, F. Applications of CRISPR–Cas systems in neuroscience. *Nat Rev Neurosci* **17**, 36–44 (2016).
2. The SCGE Consortium *et al.* The NIH Somatic Cell Genome Editing program. *Nature* **592**, 195–204 (2021).
3. Jinek, M. *et al.* A Programmable Dual-RNA–Guided DNA Endonuclease in Adaptive Bacterial Immunity. *Science* **337**, 816–821 (2012).
4. Jinek, M. *et al.* RNA-programmed genome editing in human cells. *eLife* **2**, e00471 (2013).
5. Doudna, J. A. The promise and challenge of therapeutic genome editing. *Nature* **578**, 229–236 (2020).
6. Hadaczek, P. *et al.* Transduction of Nonhuman Primate Brain with Adeno-Associated Virus Serotype 1: Vector Trafficking and Immune Response. *Human Gene Therapy* **20**, 225–237 (2009).
7. Ciesielska, A. *et al.* Cerebral Infusion of AAV9 Vector-encoding Non-self Proteins Can Elicit Cell-mediated Immune Responses. *Molecular Therapy* **21**, 158–166 (2013).
8. Samaranch, L. *et al.* AAV9-mediated Expression of a Non-self Protein in Nonhuman Primate Central Nervous System Triggers Widespread Neuroinflammation Driven by Antigen-presenting Cell Transduction. *Molecular Therapy* **22**, 329–337 (2014).
9. Agustín-Pavón, C., Mielcarek, M., Garriga-Canut, M. & Isalan, M. Deimmunization for gene therapy: host matching of synthetic zinc finger constructs enables long-term mutant Huntingtin repression in mice. *Mol Neurodegeneration* **11**, 64 (2016).

893 10. Chew, W. L. *et al.* A multifunctional AAV–CRISPR–Cas9 and its host response. *Nat Methods*
894 **13**, 868–874 (2016).
895 11. Moreno, A. M. *et al.* immune-orthogonal orthologues of AAV capsids and of Cas9
896 circumvent the immune response to the administration of gene therapy. *Nat Biomed Eng* **3**,
897 806–816 (2019).
898 12. Li, A. *et al.* AAV-CRISPR Gene Editing Is Negated by Pre-existing Immunity to Cas9.
899 *Molecular Therapy* **28**, 1432–1441 (2020).
900 13. Simhadri, V. L. *et al.* Prevalence of Pre-existing Antibodies to CRISPR-Associated Nuclease
901 Cas9 in the USA Population. *Molecular Therapy - Methods & Clinical Development* **10**, 105–
902 112 (2018).
903 14. Charlesworth, C. T. *et al.* Identification of preexisting adaptive immunity to Cas9 proteins in
904 humans. *Nat Med* **25**, 249–254 (2019).
905 15. Wagner, D. L. *et al.* High prevalence of Streptococcus pyogenes Cas9-reactive T cells within
906 the adult human population. *Nat Med* **25**, 242–248 (2019).
907 16. Ferdosi, S. R. *et al.* Multifunctional CRISPR-Cas9 with engineered immunosilenced human T
908 cell epitopes. *Nat Commun* **10**, 1842 (2019).
909 17. Tang, X.-Z. E., Tan, S. X., Hoon, S. & Yeo, G. W. Pre-existing adaptive immunity to the RNA-
910 editing enzyme Cas13d in humans. *Nat Med* **28**, 1372–1376 (2022).
911 18. Mingozzi, F. & High, K. A. Immune responses to AAV vectors: overcoming barriers to
912 successful gene therapy. *Blood* **122**, 23–36 (2013).
913 19. Staahl, B. T. *et al.* Efficient genome editing in the mouse brain by local delivery of
914 engineered Cas9 ribonucleoprotein complexes. *Nat Biotechnol* **35**, 431–434 (2017).

915 20. Liu, J., Gaj, T., Wallen, M. C. & Barbas, C. F. Improved Cell-Penetrating Zinc-Finger Nuclease
916 Proteins for Precision Genome Engineering. *Molecular Therapy - Nucleic Acids* **4**, e232
917 (2015).
918 21. Madisen, L. *et al.* A robust and high-throughput Cre reporting and characterization system
919 for the whole mouse brain. *Nat Neurosci* **13**, 133–140 (2010).
920 22. Oura, S. *et al.* Precise CAG repeat contraction in a Huntington's Disease mouse model is
921 enabled by gene editing with SpCas9-NG. *Commun Biol* **4**, 771 (2021).
922 23. Ran, F. A. *et al.* In vivo genome editing using Staphylococcus aureus Cas9. *Nature* **520**, 186–
923 191 (2015).
924 24. Maeder, M. L. *et al.* Development of a gene-editing approach to restore vision loss in Leber
925 congenital amaurosis type 10. *Nat Med* **25**, 229–233 (2019).
926 25. Yin, C. *et al.* In Vivo Excision of HIV-1 Provirus by saCas9 and Multiplex Single-Guide RNAs in
927 Animal Models. *Molecular Therapy* **25**, 1168–1186 (2017).
928 26. Gao, G. *et al.* Clades of Adeno-Associated Viruses Are Widely Disseminated in Human
929 Tissues. *J Virol* **78**, 6381–6388 (2004).
930 27. Smith, R. H., Levy, J. R. & Kotin, R. M. A Simplified Baculovirus-AAV Expression Vector
931 System Coupled With One-step Affinity Purification Yields High-titer rAAV Stocks From
932 Insect Cells. *Molecular Therapy* **17**, 1888–1896 (2009).
933 28. Chen, C., Akerstrom, V., Baus, J., Lan, M. S. & Breslin, M. B. Comparative analysis of the
934 transduction efficiency of five adeno associated virus serotypes and VSV-G pseudotype
935 lentiviral vector in lung cancer cells. *Virol J* **10**, 86 (2013).

936 29. Gaj, T. *et al.* Targeted gene knock-in by homology-directed genome editing using Cas9
937 ribonucleoprotein and AAV donor delivery. *Nucleic Acids Research* **45**, e98–e98 (2017).
938 30. Park, I.-H. *et al.* Reprogramming of human somatic cells to pluripotency with defined
939 factors. *Nature* **451**, 141–146 (2008).
940 31. Qi, Y. *et al.* Combined small-molecule inhibition accelerates the derivation of functional
941 cortical neurons from human pluripotent stem cells. *Nat Biotechnol* **35**, 154–163 (2017).
942 32. Chambers, S. M. *et al.* Highly efficient neural conversion of human ES and iPS cells by dual
943 inhibition of SMAD signaling. *Nat Biotechnol* **27**, 275–280 (2009).
944 33. Fu, Y. *et al.* High-frequency off-target mutagenesis induced by CRISPR-Cas nucleases in
945 human cells. *Nat Biotechnol* **31**, 822–826 (2013).
946 34. Bobo, R. H. *et al.* Convection-enhanced delivery of macromolecules in the brain. *Proc. Natl.*
947 *Acad. Sci. U.S.A.* **91**, 2076–2080 (1994).
948 35. Hadaczek, P. *et al.* Convection-Enhanced Delivery of Adeno-Associated Virus Type 2 (AAV2)
949 into the Striatum and Transport of AAV2 Within Monkey Brain. *Human Gene Therapy* **17**,
950 291–302 (2006).
951 36. Hanlon, K. S. *et al.* High levels of AAV vector integration into CRISPR-induced DNA breaks.
952 *Nat Commun* **10**, 4439 (2019).
953 37. Nelson, C. E. *et al.* Long-term evaluation of AAV-CRISPR genome editing for Duchenne
954 muscular dystrophy. *Nat Med* **25**, 427–432 (2019).
955 38. Ferrari, S. *et al.* Choice of template delivery mitigates the genotoxic risk and adverse impact
956 of editing in human hematopoietic stem cells. *Cell Stem Cell* **29**, 1428-1444.e9 (2022).

957 39. Simpson, B. P., Yrigollen, C. M., Izda, A. & Davidson, B. L. Targeted long-read sequencing
958 captures CRISPR editing and AAV integration outcomes in brain. *Molecular Therapy*
959 S1525001623000047 (2023) doi:10.1016/j.ymthe.2023.01.004.
960 40. Zink McCullough, K. *Calculating Endotoxin Limits for Drug Products*.
961 https://www.acciusa.com/pdfs/supplements/Endotoxin%20Detection%20Part%20VI/Calcul
962 ating_Endotoxin_Limits.pdf.
963 41. Lee, B. *et al.* Nanoparticle delivery of CRISPR into the brain rescues a mouse model of fragile
964 X syndrome from exaggerated repetitive behaviours. *Nat Biomed Eng* **2**, 497–507 (2018).
965 42. Park, H. *et al.* In vivo neuronal gene editing via CRISPR–Cas9 amphiphilic nanocomplexes
966 alleviates deficits in mouse models of Alzheimer's disease. *Nat Neurosci* **22**, 524–528
967 (2019).
968 43. Metzger, J. M. *et al.* Efficient in vivo neuronal genome editing in the mouse brain using
969 nanocapsules containing CRISPR-Cas9 ribonucleoproteins. *Biomaterials* **293**, 121959 (2023).
970 44. Wang, Y. *et al.* Overcoming the Blood–Brain Barrier for Gene Therapy via Systemic
971 Administration of GSH-Responsive Silica Nanocapsules. *Advanced Materials* 2208018 (2022)
972 doi:10.1002/adma.202208018.
973 45. Yan, S. *et al.* Cas9-mediated replacement of expanded CAG repeats in a pig model of
974 Huntington's disease. *Nat. Biomed. Eng* (2023) doi:10.1038/s41551-023-01007-3.
975 46. He, M. *et al.* A traceless linker for aliphatic amines that rapidly and quantitatively fragments
976 after reduction. *Chem. Sci.* **11**, 8973–8980 (2020).
977 47. Sweeney, M. D., Sagare, A. P. & Zlokovic, B. V. Blood–brain barrier breakdown in Alzheimer
978 disease and other neurodegenerative disorders. *Nat Rev Neurol* **14**, 133–150 (2018).

979 48. Huang, L. *et al.* Expression of tdTomato and luciferase in a murine lung cancer alters the
980 growth and immune microenvironment of the tumor. *PLoS ONE* **16**, e0254125 (2021).
981 49. Tsai, S. Q. *et al.* GUIDE-seq enables genome-wide profiling of off-target cleavage by CRISPR-
982 Cas nucleases. *Nat Biotechnol* **33**, 187–197 (2015).
983 50. Tsai, S. Q. *et al.* CIRCLE-seq: a highly sensitive in vitro screen for genome-wide CRISPR–Cas9
984 nuclease off-targets. *Nat Methods* **14**, 607–614 (2017).
985 51. Ibraheim, R. *et al.* Self-inactivating, all-in-one AAV vectors for precision Cas9 genome
986 editing via homology-directed repair in vivo. *Nat Commun* **12**, 6267 (2021).
987 52. Li, A. *et al.* A Self-Deleting AAV-CRISPR System for In Vivo Genome Editing. *Mol Ther*
988 *Methods Clin Dev* **12**, 111–122 (2019).
989 53. Merienne, N. *et al.* The Self-Inactivating KamiCas9 System for the Editing of CNS Disease
990 Genes. *Cell Rep* **20**, 2980–2991 (2017).
991 54. Ewaisha, R. & Anderson, K. S. Immunogenicity of CRISPR therapeutics—Critical
992 considerations for clinical translation. *Front. Bioeng. Biotechnol.* **11**, 1138596 (2023).
993 55. Bae, S., Park, J. & Kim, J.-S. Cas-OFFinder: a fast and versatile algorithm that searches for
994 potential off-target sites of Cas9 RNA-guided endonucleases. *Bioinformatics* **30**, 1473–1475
995 (2014).
996 56. Clement, K. *et al.* CRISPResso2 provides accurate and rapid genome editing sequence
997 analysis. *Nat Biotechnol* **37**, 224–226 (2019).
998 57. Martin, M. Cutadapt removes adapter sequences from high-throughput sequencing reads.
999 *EMBnet j.* **17**, 10 (2011).

1000 58. Sedlazeck, F. J. *et al.* Accurate detection of complex structural variations using single-
1001 molecule sequencing. *Nat Methods* **15**, 461–468 (2018).
1002 59. Ramírez, F. *et al.* High-resolution TADs reveal DNA sequences underlying genome
1003 organization in flies. *Nat Commun* **9**, 189 (2018).
1004 60. Lopez-Delisle, L. *et al.* pyGenomeTracks: reproducible plots for multivariate genomic
1005 datasets. *Bioinformatics* **37**, 422–423 (2021).
1006
1007

Figure Legends

Figure 1. In vivo editing at tdTomato locus with viral and non-viral Cas9 delivery strategies. (A) Schematic of 4x-SpyCas9-2x cell-penetrating protein expression and purification systems, (B) AAV9-SauCas9-sgRNA expression and purification systems, (C) and expected edited brain regions in the partial basal ganglia direct circuit shown in sagittal view (top) and coronal view (bottom). Neurons extend from the striatum into the globus pallidus (GP) and substantia nigra (SNr). Created with BioRender.com. (D) Comparison of standard blunt ended needles versus those fitted with CED cannula had a similar amount of edited striatal volume and markers of tissue damage (supplement), however the CED needle significantly reduced reflux of RNP back up the needle injection track (n=3-6 injections per group, ** $p<0.01$.) Scale bar:1 mm. (E) Serial sections of single hemisphere sagittal view of edited tdTomato+ cells in the basal ganglia circuit after injection of Cas9 RNP with CED into the striatum, with signal detected near the GP and SNr. Scale bar: 1 mm. (F) Representative coronal section of the striatum of mice that received Cas9 RNPs and AAVs at 21 days post-injection, showing the distribution of tdTomato+ edited cells. Scale bar: 1 mm. (G) Co-staining of tdTomato with NeuN and GFAP showed that neurons were the predominately edited cell type in the striatum (>99% of tdTomato+ cells in the edited region of interest co-expressed NeuN in Cas9 AAV and Cas9 RNP at 125pmol). However, at doses of Cas9 RNPs greater than 125pmol, a decrease in NeuN staining and an increase in GFAP staining was observed out to 90-days. Scale bar: 50 µm. (H) The volume of edited striatal tissue was stable as the concentration of injected Cas9 RNPs was increased from 10 to 100 µM (n=4-6 injections). Since 125pmol dose had the highest maximal level of detected editing, we proceeded with this dose for subsequent studies. (I) Cas9 AAV had significantly greater edited striatal tissue than Cas9 RNPs at 125pmol dose at 21 and 90-days post-injection (n=4-6 injections, * $p< 0.05$). (J) Within the region of interest (ROI) Cas9 RNPs

edited approximately 36% of NeuN+ neurons, while Cas9 AAV edited approximately 20% of neurons. Scale bar: 250 µm.

Figure 2. Immune response to in vivo editing with viral and non-viral Cas9 delivery strategies. (A) Representative immunostaining of Iba1 (microglia, green) with tdTomato and DAPI using confocal microscopy. Scale bar: 50 µm. (B) Quantification of Iba1$^+$ cells, staining intensity, and percent area (n=4-6 technical replicates, one-way ANOVA, *p<0.05). (C) Quantification of CD45$^+$ and CD3$^+$ cells per image (n=3-6 replicates, one-way ANOVA, ns) with representative confocal images. (D) Representative images of CD45, CD3, and Iba1 showing co-expression of CD45 (green) with both Iba1 (microglia, red) and CD3 (T-cells, red) cells and differential cell morphology. Merged images include DAPI (gray) and tdTomato (magenta). Scale bar: 50 µm. (E) Quantification of IgG antibodies against Cas9 or AAV capsid proteins measured 28 and 90-days after bilateral intrastriatal injections by ELISA (n=3-5 biological replicates). (F) Heat map summarizing RT-qPCR results of 21 genes at two time-points. At each time point, Ppih was used as a housekeeping control for delta-delta Ct analysis and compared to the sham group using Qiagen analysis portal (n=4, *p < 0.05).

Figure 3. Optimized, low-endotoxin RNP formulation reduces local immune response. (A) Schematic of manufacturing scale up to produce industrial quantity of ultra-low endotoxin 4x-SpyCas9-2x protein using a tag-free expression and purification system. (B) Endotoxin levels calculated on a per mouse basis between the standard (laboratory 4x-SpyCas9-2x with sg298 2018) and optimized (industrial 4x-SpyCas9-2x protein with sg298 2022) RNP formulations at 25µM measured by LAL assay. The optimized RNP had a final endotoxin level of 0.44 EU/kg, just above the FDA recommendation of 0.2 EU/kg/hr (dotted line) for human drug products administered into the central nervous system. (C) Quantification of Iba1$^+$ staining intensity and

percent area (n=6-10, one-way ANOVA, *$p<0.05$). (D) Quantification of $CD45^+$ and (E) $CD3^+$ cells per image (n=6-10, one-way ANOVA, ns). (F) Percent volume of edited striatal tissue for Cas9 RNPs injected at 25µM (n=6-10 injections). (G) Quantification of IgG antibodies against Cas9 or AAV capsid proteins measured 21-days after bilateral intrastriatal injections by ELISA (n=3-5 biological replicates).

Figure 1. In vivo editing at tdTomato locus with viral and non-viral Cas9 delivery strategies

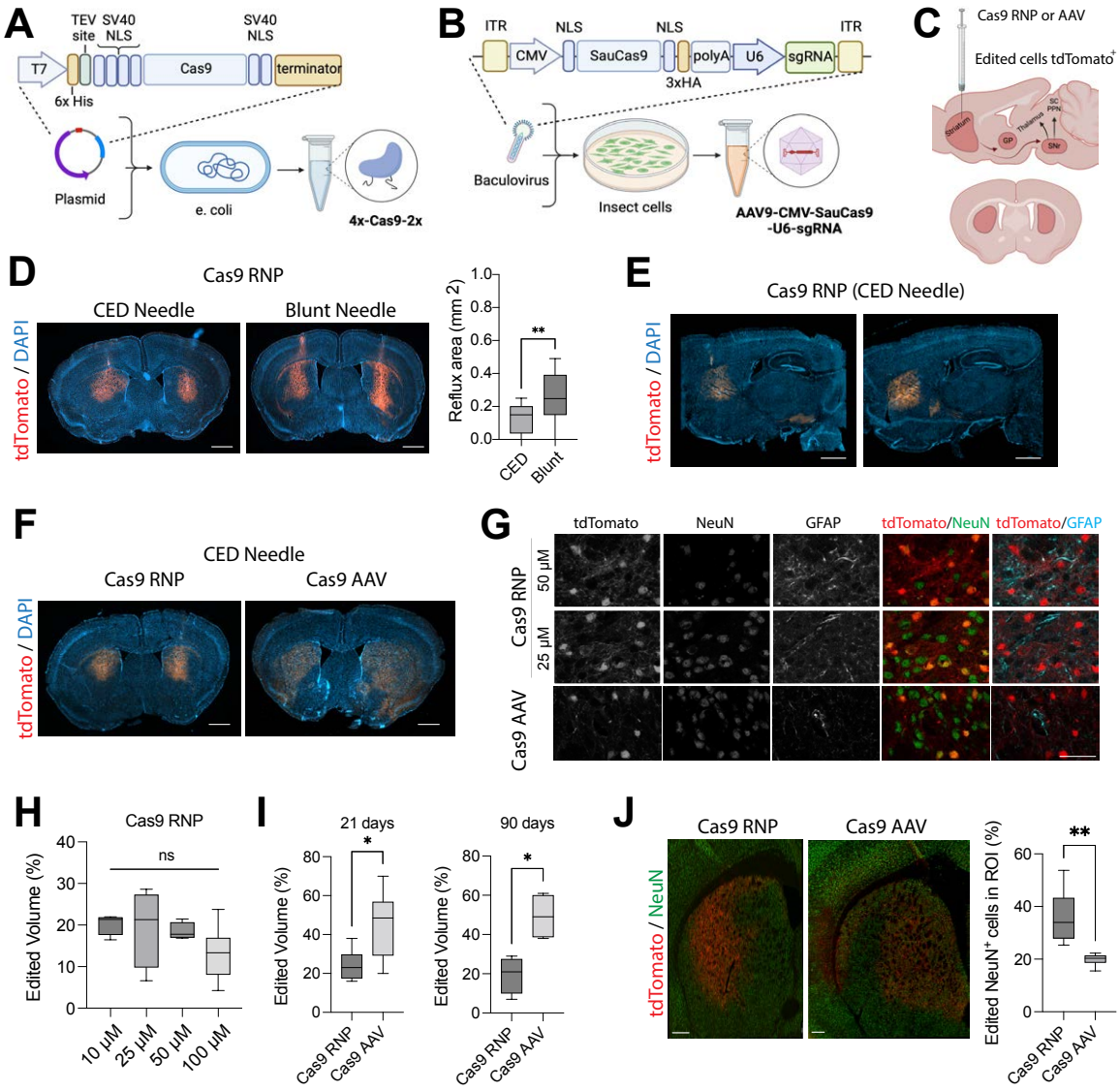

Figure 2. Immune response to in vivo editing with viral and non-viral Cas9 delivery strategies

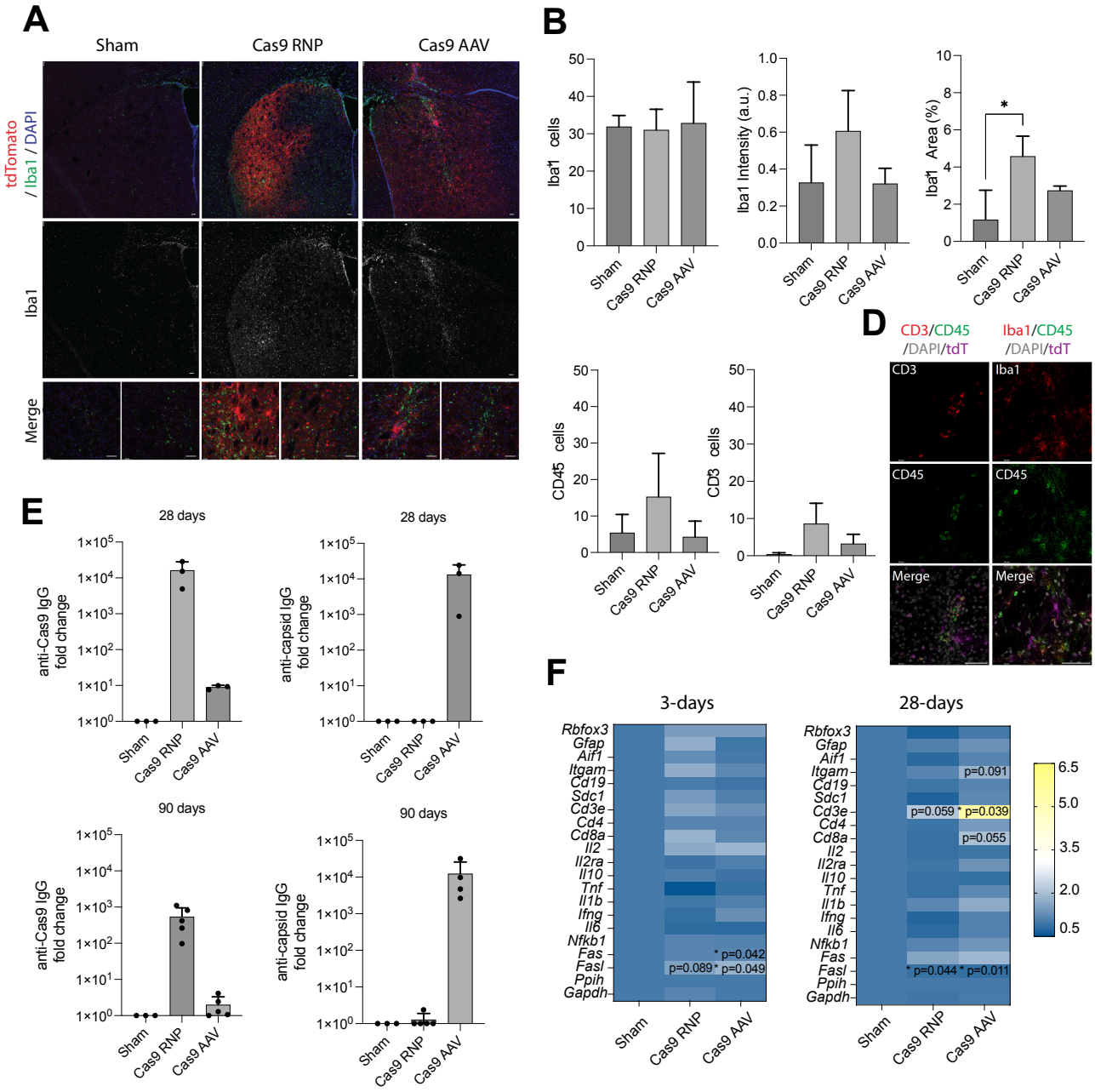
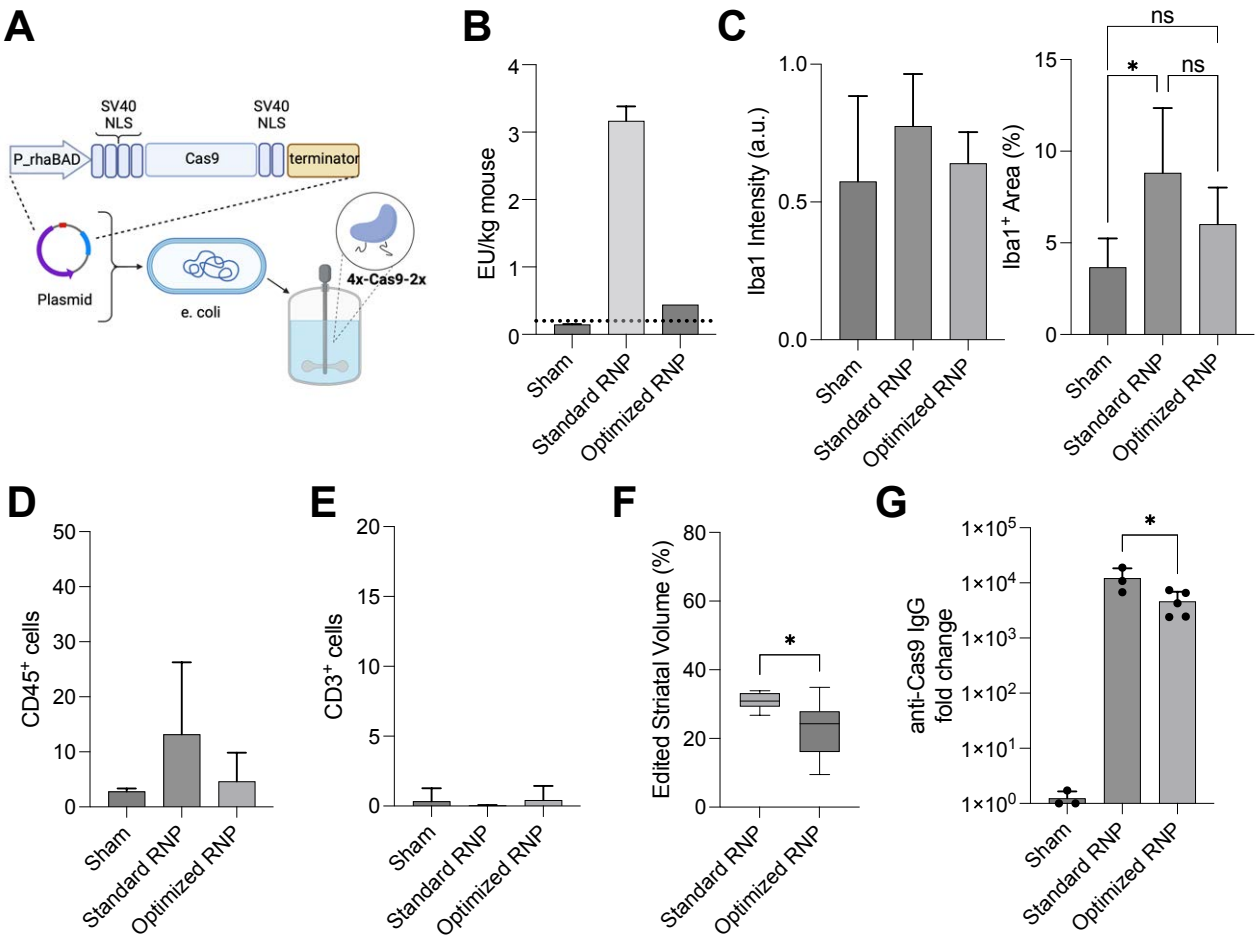
Figure 3. Optimized, low-endotoxin RNP formulation reduces local immune response